

**Size and transparency influence diel vertical  
migration patterns in copepods.**

Alex Barth<sup>\*1</sup>, Rod Johnson<sup>2</sup> and Joshua Stone<sup>1</sup>

1. University of South Carolina, Biological Sciences, 700 Sumter St  
401, Columbia, SC 29208
2. Bermuda Institute of Ocean Sciences, Bermuda GE 01, UK

<sup>2</sup> **0.1 Scientific Significance Statement**

<sup>3</sup> **0.1.1 Study Novelty**

<sup>4</sup> Diel Vertical Migration is a widespread phenomenon across marine and fresh-  
<sup>5</sup> water systems. The predator evasion hypothesis suggests that DVM occurs as  
<sup>6</sup> zooplankton attempt to escape visual predators. Yet, DVM itself is a costly  
<sup>7</sup> and risky behavior. Thus, DVM should only occur when visual risk is high.  
<sup>8</sup> Several studies have shown that copepod size influences the magnitude of DVM.  
<sup>9</sup> However, an individual's visual risk may include traits beyond simply size. In  
<sup>10</sup> this study, we utilize an in-situ imaging tool to reveal how copepod morpholog-  
<sup>11</sup> ical traits influence DVM. Our findings show that both size and transparency  
<sup>12</sup> influence DVM. We support this finding through rigorous statistical analyses  
<sup>13</sup> and state-of-the-art technology. This finding provides support for leading DVM  
<sup>14</sup> hypotheses and highlights that DVM is a complex behavior driven by multiple  
<sup>15</sup> copepod traits. Furthermore, this study represents a novel application of in-situ  
<sup>16</sup> imaging technology to address major hypotheses in biological oceanography.

<sup>17</sup> **0.1.2 Applicability to L&O**

<sup>18</sup> This study addresses diel vertical migration, an active, major research topic in  
<sup>19</sup> biological oceanography. Many studies published in L&O contribute to advanc-  
<sup>20</sup> ing knowledge on DVM. In this paper, we provide strong evidence for both size  
<sup>21</sup> and transparency influencing DVM behavior. Additionally, we accomplished  
<sup>22</sup> this study using emerging technology and statistical analyses. This work builds  
<sup>23</sup> on research published in L&O and will be broadly applicable to plankton ecol-

<sup>24</sup> ogists, biological oceanographers.

<sup>25</sup> AB and JS developed the study hypotheses. JS coordinated deployment and  
<sup>26</sup> data management of the UVP. RJ facilitated data collection on cruises. AB  
<sup>27</sup> led the analysis and preparation of the manuscript and figures. JS and RJ  
<sup>28</sup> contributed to the manuscript draft. All authors approved the final submission.

## <sup>29</sup> 1 Abstract

<sup>30</sup> Diel vertical migration (DVM) is a widespread phenomenon in aquatic environments.  
<sup>31</sup> The primary hypothesis explaining DVM is the visual predator evasion hypothesis,  
<sup>32</sup> which suggests that zooplankton migrate to deeper waters to avoid detection during daylight.  
<sup>33</sup> However, visual risk also depends on a copepod's morphology. In this study, we investigate hypotheses related to morphology and DVM: (H1) size increases visual risk and will increase DVM depth and  
<sup>34</sup> (H2) copepod transparency will reduce visual risk and thus reduce DVM depth.

<sup>37</sup> In-situ Copepod images were collected across several cruises in the Sargasso Sea  
<sup>38</sup> using an Underwater Vision Profiler 5. Copepod morphology was characterized  
<sup>39</sup> from these images and a dimension reduction approach. The results show a clear  
<sup>40</sup> relationship in which larger copepods have a larger DVM signal. Darker copepods  
<sup>41</sup> also have a larger DVM signal, however only amongst the largest group of  
<sup>42</sup> copepods. This suggests multiple morphological traits influence copepod DVM  
<sup>43</sup> behavior.

<sup>44</sup> **2 Introduction**

<sup>45</sup> Diel vertical migration (DVM) is a wide spread phenomena with large conse-  
<sup>46</sup> quences in ocean ecosystems. DVM is the process of pelagic organisms verti-  
<sup>47</sup> cally moving in the water column on a daily basis, often travelling dozens to  
<sup>48</sup> hundreds of meters (Bianchi and Mislan 2016). This large-scale event occurs  
<sup>49</sup> across many taxa, from plankton to fish (Brierley 2014). However, DVM is  
<sup>50</sup> particularly notable in zooplankton communities, whose migrations contribute  
<sup>51</sup> substantially to biogeochemical cycles (Steinberg and Landry 2017; Archibald  
<sup>52</sup> et al. 2019; Siegel et al. 2023). Zooplankton communities, largely dominated  
<sup>53</sup> by copepods (Turner 2004), will feed in surface layers of the ocean at night then  
<sup>54</sup> migrate into deeper waters during daytime. Through this movement, copepods  
<sup>55</sup> actively transport carbon to depth. Additionally, Kelly et al. (2019) described  
<sup>56</sup> zooplankton DVM to be a major component of mesopelagic food webs. Thus to  
<sup>57</sup> understand pelagic food webs and nutrient cycles, it is critically important to  
<sup>58</sup> understand the drivers of DVM.

<sup>59</sup> Predominantly, zooplankton DVM is the movement from deep waters at daytime  
<sup>60</sup> to shallower waters at night (Hays 2003; Bianchi and Mislan 2016). The leading  
<sup>61</sup> explanation for this pattern is the predator-avoidance hypothesis (Bandara et al.  
<sup>62</sup> 2021). This hypothesis posits zooplankton evacuate the sunlit surface to evade  
<sup>63</sup> visual predators then ascend at night to feed. However, the massive migration  
<sup>64</sup> undertaken by these copepods is energetically expensive (Maas et al. 2018; Robi-  
<sup>65</sup> son et al. 2020). Therefore, the visual predator evasion hypothesis implies that

66 DVM is a result of visual risk exceeding migration costs. However, a copepod's  
67 visual risk to a visual predator depends on morphological features (Aksnes and  
68 Utne 1997). Notably a copepod's size can increase visual detection. Several  
69 studies have documented that copepod size influences DVM magnitude (Hays  
70 et al. 1994; Aarflot et al. 2019). Presumably, a copepod's transparency will  
71 also influence DVM. Hays et al. (1994) reported that pigmentation explained  
72 variation in DVM frequency. However, few other studies have investigated this  
73 at length. One barrier to studying a relationship between copepod morphology  
74 and DVM is the difficulty of accurately recording traits.

75 In-situ imaging tools offer great potential to better describe copepod DVM. By  
76 directly observing copepods, new insights into their behavior and traits can be  
77 resolved (Ohman 2019). For example, Whitmore and Ohman (2021) used an  
78 in-situ imaging device to describe a relationship between copepod abundance  
79 with a particulate field rather than chlorophyll-a. Such findings are facilitated  
80 by the fact imagery data records an individual's exact position. Additionally, a  
81 copepod's true appearance can be documented whereas net-collected organisms  
82 are often physically deformed or lacking color due to decomposition or preserva-  
83 tion. Some studies have noted a copepod DVM with in-situ imagery data (Pan  
84 et al. 2018; Whitmore and Ohman 2021). However, direct tests of DVM-related  
85 hypotheses with such data have not been conducted.

86 In this study, we utilized in-situ imaging to evaluate how copepod morphologi-  
87 cal traits influence patterns. We specifically test the hypotheses that, (H1) size  
88 increases visual risk and will increase DVM magnitude and (H2) copepod trans-

89 parency will reduce visual risk and thus reduce DVM. If these morphologically  
90 based hypotheses are true, then the larger and darker copepods will have the  
91 largest DVM signals.

### 92 3 Methods

#### 93 3.1 CTD profiles and UVP imaging of copepods

94 Data were collected aboard the R/V Atlantic Explorer in collaboration with the  
95 Bermuda Atlantic Time-series Study (BATS) (Steinberg et al. 2001). In-situ  
96 images of plankton were acquired using an Underwater Vision Profiler (UVP5)  
97 (Picheral et al. 2010). The original sampling methodology and instrument  
98 specification followed details described in Barth and Stone (2022). The UVP was  
99 attached to the CTD rosette and deployed regularly on cruises to the Sargasso  
100 Sea from June 2019 - December 2021. Typical monthly cruises included ~13  
101 profiles with average descents to 1200m (Supplemental Figure 1). In this study,  
102 we investigated general trends in DVM by pooling together casts across multiple  
103 cruises. This approach is necessitated by the small sampling volume of the UVP  
104 and low abundance of plankton which requires aggregation of data to resolve  
105 trends (Barth and Stone 2022). While there was some variation between cruises  
106 (Supplemental Figure 2), this oligotrophic system is relatively consistent across  
107 seasons (Steinberg et al. 2001). Additionally, every cruise had an approximately  
108 equal number of day and night casts. Profiles were assigned to be day or night  
109 based on locally calculated nautical dawn and nautical dusk times using the R

110 package **suncalc** 0.5.1.

111 The UVP records images of large particles ( $>600\mu\text{m}$  equivalent spherical diam-  
112 eter, ESD). However, living particles are not reliably identifiable below  $900\mu\text{m}$   
113 (Barth and Stone 2022). All recorded images were processed using Zooprocess  
114 (Gorsky et al. 2010), which provides several metrics related to size, grey value,  
115 and shape complexity. These features were then used to automatically sort  
116 images using Ecotaxa (Picheral et al.). All images were manually verified by  
117 the same trained taxonomist. In total, 294,913 images were recorded. Of these,  
118 85.2% were images of debris or artefacts. The smallest identified copepod was  
119 0.940mm ESD and the largest was 5.904mm ESD. Across all casts, copepods  
120 were the most common organism, composing 58.7% of all identified, living par-  
121 ticles. In total, there were 4151 individual copepods images.

### 122 3.2 Morphological Grouping

123 Zooprocess measures and collects several morphologically relevant parameters.  
124 To create relevant groups of copepods, a dimension reduction approach was  
125 used. Similar methods have been successfully utilized to provide novel insights  
126 to marine snow (Trudnowska et al. 2021), copepod dynamics in the Arctic  
127 (Vilgrain et al. 2021), and temporal trends in phytoplankton communities (Son-  
128 net et al. 2022). First, 18 morphologically relevant parameters were selected  
129 to be included in a principal Components Analysis (PCA), following (Vilgrain  
130 et al. 2021). Parameters can be described as relating to size (e.g. major axis,  
131 feret diameter, ESD), grey intensity (e.g. mean grey value at 625nm wavelength

132 light), shape (e.g. elongation, symmetry), and shape complexity (e.g. fractal  
133 dimension). The PCA was weighted by the volume sampled in a 1-m depth bin  
134 for each observation. This approach provides a correction for the UVP's vari-  
135 able descent speed which can cause duplicate imaging of individuals. While this  
136 phenomena has a minor impact on overall results (Barth and Stone 2022), we  
137 used the weighted approach to assure that no individual features were overrepre-  
138 sented. All morphological descriptors were scaled and centered prior to inclusion  
139 in the analysis. The model was constructed using the R package **FactoMineR**  
140 2.7. principal components were deemed to be significant if their eigenvalues  
141 were greater than 1. This approach yielded 4 PCs which described 87.3% of the  
142 total variation in morphological parameters, with 34.5% and 26.5% in the first  
143 two components respectively. This four principal component space provides a  
144 “morphospace” to characterize copepods.

145 To address our morphology-DVM hypotheses, we constructed discrete morpho-  
146 logical groups based on the first two principal components. Groups along each  
147 of the principal components were defined as low (below 25th percentile), mid  
148 (25th-75th percentile) and high (greater than 75th percentile). To address the  
149 size-dependent hypothesis (H1), groups were assigned as low, mid, or high along  
150 PC1. Then to assess if color/transparency was a secondary factor (H2), within  
151 each PC1 group, PC2 groups were constructed as low, mid, or high. In total,  
152 this created 9 groups (e.g. Low PC1-Low PC2, Low P1-mid PC2, etc).

153 **3.3 Copepod vertical structure & DVM**

154 **3.3.1 Vertical distribution of copepods**

155 Copepods in this system are well documented to undergo DVM (Steinberg et  
156 al. 2000; Schnetzer and Steinberg 2002; Maas et al. 2018). However, there  
157 have not been direct measurements of DVM with in-situ imaging data. First, to  
158 assess which portion of the water column copepods were utilizing for DVM, we  
159 visualized the average vertical structure. The concentrations of each morpholog-  
160 ical group (based on PC1 and PC2) were calculated in 20m depth bins for each  
161 UVP profile. Profiles were designated as either day or night. Then across all  
162 day/night profiles, the mean concentration was calculated for each 20m depth  
163 bin.

164 **3.3.2 Weighted mean depth variability**

165 Weighted mean depth (WMD) is a common metric to describe vertical structure  
166 and DVM in zooplankton (Ohman et al. 2002; Ohman and Romagnan 2016;  
167 Aarflot et al. 2019). However, with in-situ imagery, this approach presents a  
168 few challenges. WMD cannot be calculated individually for each profile then  
169 averaged because each profile had a different descent depth. Additionally, the  
170 small and uneven sampling volume of the UVP can make single casts too vari-  
171 able to reliably resolve abundance. Yet, understanding variation around the  
172 WMD is necessary to compare DVM strength across groups. Here, we intro-  
173 duce a depth-bin constrained bootstrap approach to define WMD with a 95%  
174 confidence interval. To do this, the concentration of each group, was calculated

175 in 20m depth bins for each profile. Then all profiles were ‘pooled’, separately  
 176 for day/night. This provides a distribution of concentrations in each depth-bin.  
 177 However, due to the different descent speeds and depth of profiles, there are  
 178 more observations of surface depth bins. Thus, traditional bootstrapping would  
 179 bias estimate toward the surface as resampling would be more likely to draw  
 180 a more-frequently observed surface bin. To avoid this, bootstrap samples were  
 181 “bin-constrained” such that for each iteration, a random observation was drawn  
 182 within each depth bin, then replaced for the next iteration. A maximum depth  
 183 was set to 600m based on qualitative observations of vertical profiles. This ap-  
 184 proach effectively created a random profile by resampling a concentration,  $conc^*$ ,  
 185 from each depth bin,  $d$ . For each iteration, the random constructed profile then  
 186 was used to calculate a bootstrapped weighted mean depth,  $WMD^*$ . This was  
 187 done for each morphological group,  $g$ , at each time of day,  $t$  (day/night).

$$WMD_{g,t}^* = \sum_i^{N=30} \frac{d_i(conc_{i,g,t}^*)}{\sum_i^{N=30} conc_{i,g,t}^*}$$

188 The distribution of  $WMD_{g,t}^*$  then was used to calculate a bootstrapped mean  
 189 and 95% confidence interval. The 95% CIs could be compared between times  
 190 of day and morphological groups to assess the strength of DVM. Using PC1  
 191 to assess size, the WMD was compared between the three PC1-groups by per-  
 192 centile level. Then to assess the effect of transparency the WMD was compared  
 193 between PC2-groups within each PC1-grouping. A larger signal of DVM would  
 194 be evident by a clearly deeper (non-overlapping 95% CI) daytime WMD.

<sup>195</sup> **4 Results**

<sup>196</sup> **4.1 Morphological Groups**

<sup>197</sup> The PCA revealed four major axis of variability (Figure 1). The first axis (PC1,  
<sup>198</sup> 34.23% of variability) was largely explained by increasing values related to size,  
<sup>199</sup> such as perimeter (loading score = 0.927) and feret diameter (loading score =  
<sup>200</sup> 0.910). The second axis (PC2, 27.24% of variability) can be interpreted as a  
<sup>201</sup> gradient of transparent to dark individuals. PC2 was largely anticorrelated with  
<sup>202</sup> mean grey value (higher values indicate a more transparent individual) (loading  
<sup>203</sup> score = -0.920). As noted in the methods, PC3 and PC4 were both related to  
<sup>204</sup> the orientation of the copepod and the appendage visibility respectively (Sup-  
<sup>205</sup> plemental Figure 3).

<sup>206</sup> The morphological groupings were assigned along PC1 as low, mid and high.  
<sup>207</sup> Then along PC2, groups were assigned within each PC1-group (Figure 1). To  
<sup>208</sup> confirm the morphospace grouping resulted in ecologically relevant categories,  
<sup>209</sup> the morphological groups were compared against known copepod metrics.  
<sup>210</sup> Across all PC1-groups, there was a clear difference in feret diameter. The  
<sup>211</sup> median feret diameter of the low group was 1.97mm. The median feret diameter  
<sup>212</sup> of the mid and high groups were 2.84mm and 4.83mm, respectively (Figure 2A).  
<sup>213</sup> All groups were significantly different from one another (Dunn Kruskall-Wallace  
<sup>214</sup> test,  $p < 0.001$ ). PC2 groups as a whole were also significantly different from  
<sup>215</sup> one another (Dunn Krustall-wallace test,  $p < 0.001$ ). However, within each  
<sup>216</sup> PC2-group, there was a clear tendency for larger copepods (high PC1 group)

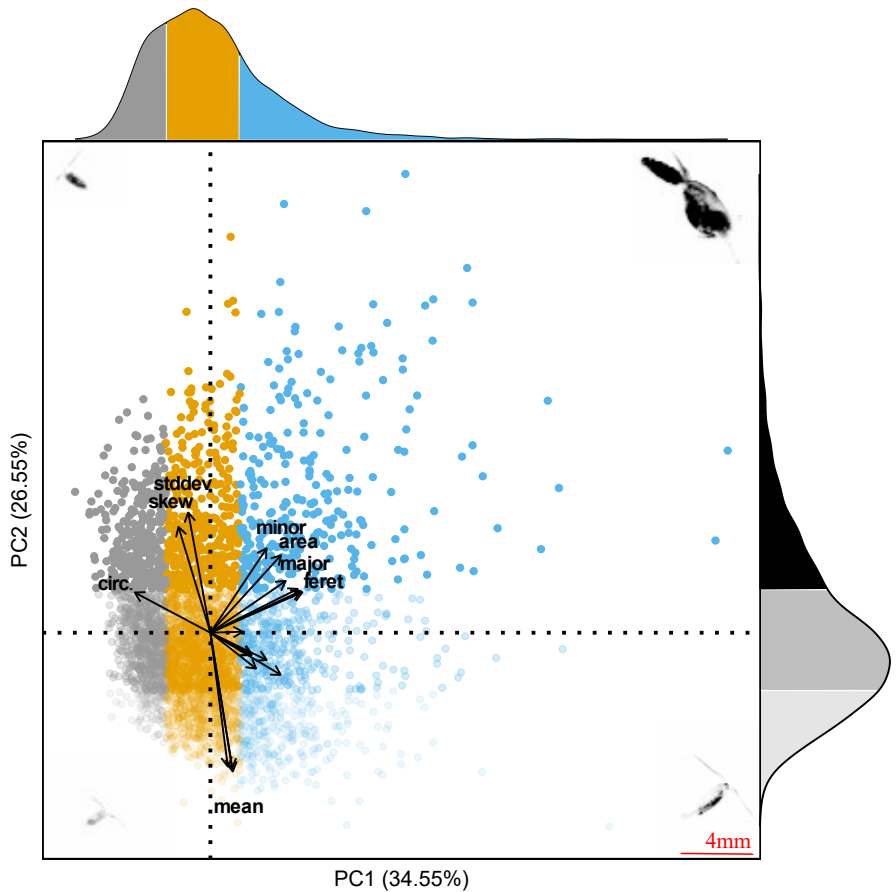


Figure 1: First two principal components of the morphospace. Proportion of variance explained by the two axis is 61.1%. Each point represents an individual copepod. The color and transparency of each point corresponds to the morphological groups based on percentile along each axis. Along PC1, grey corresponds to the low-group (<25th percentile), orange to the mid group (25th-75th percentiles), and blue to the high-group (75th percentile). Along PC2, low, mid, and high groups are distinguished by increasing opacity. Marginal distribution display the proportion of observations in each group. Representative vignettes of copepods are shown in the corners corresponding to their place in the morphospace. 4mm scale bar in the bottom right is shown for the vignettes.

<sup>217</sup> to be more transparent (Figure 2B).

## <sup>218</sup> 4.2 Vertical Profiles of Morphological Groups

<sup>219</sup> For all groups, the 20m-binned profiles show a notable structure. While cope-  
<sup>220</sup> pods were observed throughout the mesopelagic (Supplemental Figure 4), the  
<sup>221</sup> majority of day/night differences were observed above 600m (Figure 3). For  
<sup>222</sup> most morphological groups, there was a peak in nighttime concentration in the  
<sup>223</sup> lower epipelagic (50m-200m). Similarly, there was a decrease in average day-  
<sup>224</sup> time concentration over the same region. This pattern is particularly apparent  
<sup>225</sup> for the groups which are mid and high on both PCs (Figure 3B, C, E, F). Across  
<sup>226</sup> all groups, both average daytime and nighttime concentration were low in the  
<sup>227</sup> upper mesopelagic (200m-300m). Then, there was a peak in average daytime  
<sup>228</sup> concentration in the depth bins in the mid-mesopelagic (400m-600m).

## <sup>229</sup> 4.3 Weighted mean depth analysis

<sup>230</sup> The bin-constrained bootstrap approach provided a direct method to compare  
<sup>231</sup> DVM between groups. Size (PC1) had a clear effect on DVM magnitude. First,  
<sup>232</sup> for all PC1 groups, daytime WMD 95% bootstrapped confidence intervals (95%  
<sup>233</sup> CIs) were deeper and non-overlapping with the nighttime 95% CIs (Figure 4).  
<sup>234</sup> This indicates a clear DVM pattern. However, the differences in day and night  
<sup>235</sup> CIs varied between morphological groups. All PC1 groups had a similar, over-  
<sup>236</sup> lapping nighttime 95% CI in the lower epipelagic (~145m - ~200m). However,  
<sup>237</sup> there was a clear difference in the depth of the daytime 95% CIs. The small

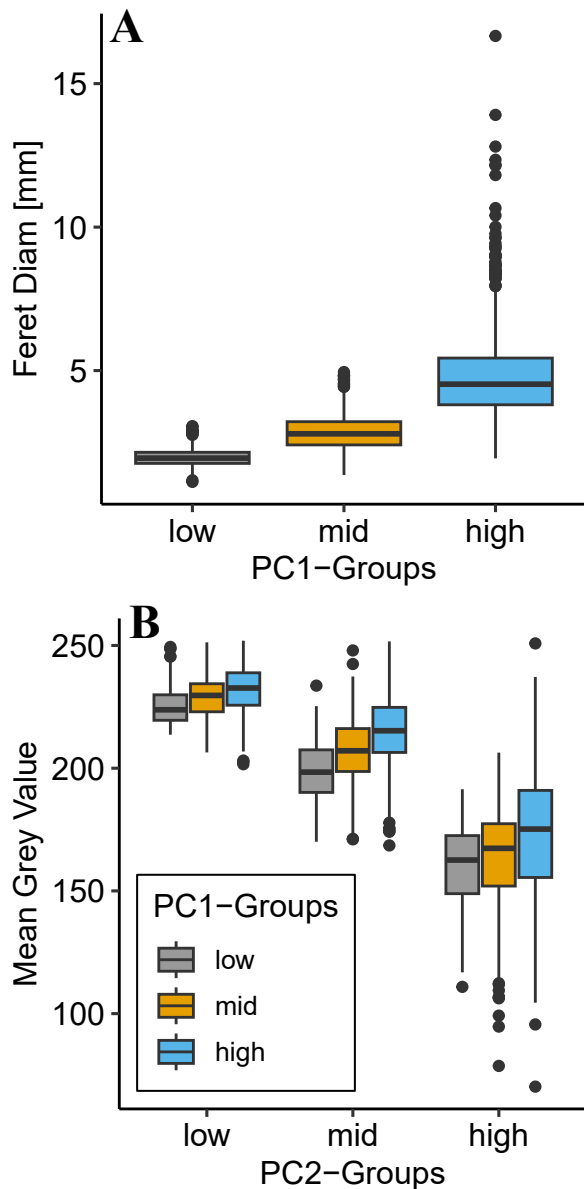


Figure 2: Comparison of morphological groups to relevant parameters. Groups were constructed along principal components with low as below 25th percentile, mid as 25th-50th percentile, and high as above 75th percentile. (A) PC1 groups are significantly different along feret diameter and display a clear trend for size. (B) PC2 groups are significantly different in terms of mean grey value. Note that a low mean grey value indicates a darker copepod.

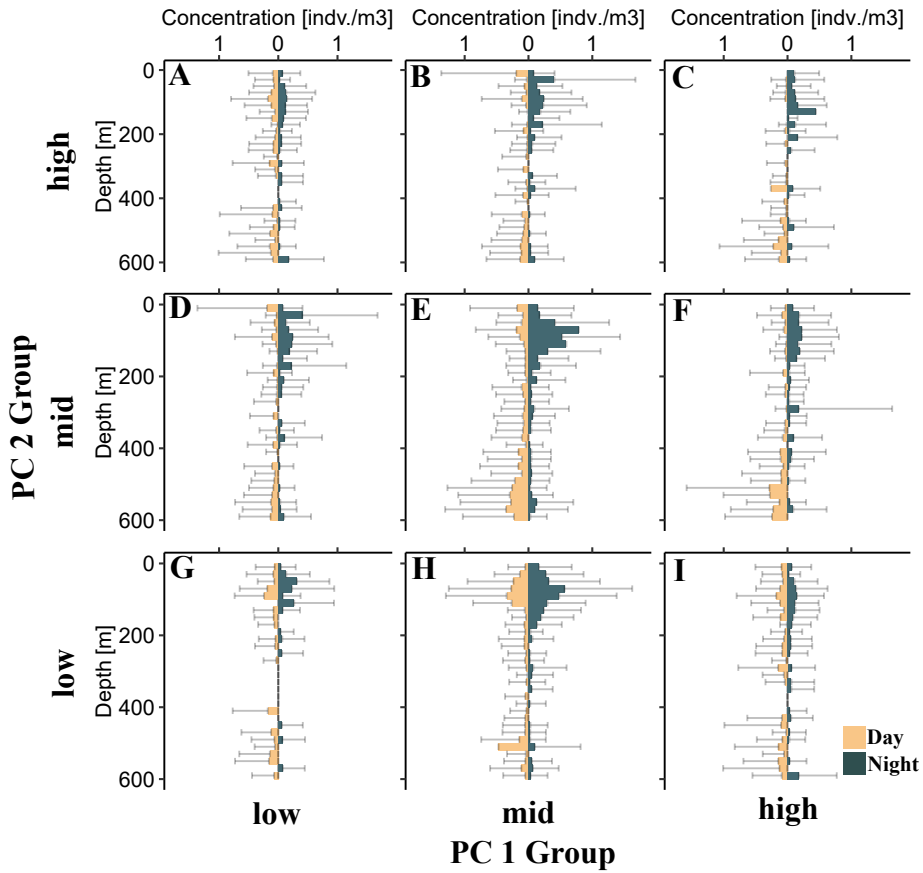


Figure 3: Average vertical profile of different copepod morphological groups. Bars display average concentration in a 20m depth bin. On each panel, left-side bars (tan) correspond to daytime while right-side (teal) bars correspond to nighttime. Standard deviation is shown for each 20m depth bin. Each panel corresponds to a morphological group along PC1 (size axis) and PC2 (transparency axis). (A) low PC1, high PC2; (B) mid PC1, high PC2; (C) high PC1, high PC2; (D) low PC1, mid PC2; (E) mid PC1, mid PC2; (F) high PC1, mid PC2; (G) low PC1, low PC2; (H) mid PC1, low PC2; (I) high PC1, low PC2

<sup>238</sup> (low PC1) group had the shallowest 95% CI (235.2m-296.0m). The mid PC1  
<sup>239</sup> group's daytime 95% CI was slightly deeper (309.0m-347.3m). The large (high  
<sup>240</sup> PC1) group daytime 95% CI was even lower (352.3m-405.0m).

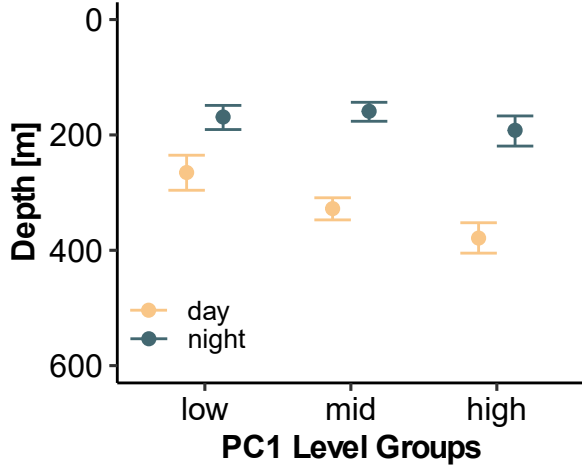


Figure 4: Mean bootstrapped weighted mean depth and 95% confidence intervals for copepods of different morphological groups. Low, mid, and high groups correspond to the different percentiles along PC1 from the morphospace. PC1 largely is explained by size metrics, with higher scores indicating a larger copepod.

<sup>241</sup> When considering the influence of transparency (PC2) on DVM magnitude, we  
<sup>242</sup> compared PC2 groups within their PC1 grouping. This approach was warranted  
<sup>243</sup> because of the tendency for size to have a slight effect on transparency (Figure  
<sup>244</sup> 2). At this level of comparison, there were several notable trends. For the  
<sup>245</sup> smaller copepods (low PC1), once the data were split into PC2 groups, the  
<sup>246</sup> wider 95% CIs indicate little to no DVM signal. Generally, the daytime 95%  
<sup>247</sup> CIs and nighttime 95% CIs are overlapping or near-overlapping (Figure 5A).  
<sup>248</sup> With mid sized copepods, there was a clear DVM signal. However, all PC2  
<sup>249</sup> groups appeared to have a similar DVM magnitude with each group's daytime

250 95% CIs overlapping with each other (Figure 5B). There was a difference in  
 251 DVM magnitude across PC2 groups within the largest copepods. The more  
 252 transparent copepods (low PC2 group) showed no DVM signal, with a shallow  
 253 daytime WMD. However, the darker copepods (mid and high PC2 groups) had  
 254 deeper daytime WMDs (Figure 5c).

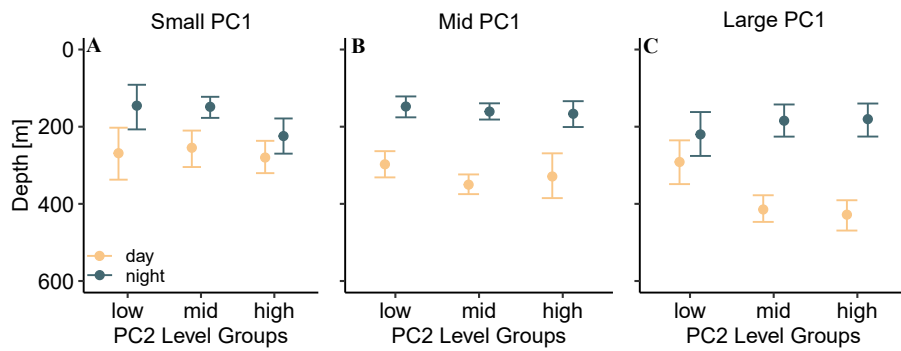


Figure 5: Mean bootstrapped weighted mean depth and 95% confidence intervals shown by copepod morphological groups along PC2 (transparency). Each panel represents a different size group of copepods (PC1 groups).

## 255 5 Discussion

### 256 5.1 Copepod morphospace

257 In this study, we built on methods for describing morphospaces from similar  
 258 in-situ imaging studies (Vilgrain et al. 2021; Trudnowska et al. 2021; Sonnet  
 259 et al. 2022). The PCA-defined morphospace with the present data aligns well  
 260 with the prior applications. Interestingly, the proportion of morphological vari-  
 261 ation explained by each axis in the morphospace defined on Arctic copepods by  
 262 Vilgrain et al. (2021) is extremely similar to the morphospace axes in this study.

263 This similarity is striking considering the vastly different copepod community  
264 compositions between the Arctic ocean and subtropical gyres (Soviadan et al.  
265 2022). The similarity of morphospaces could also be an artifact of the similarity  
266 of input data. Given the UVP has a limited range of observable size classes  
267 (Picheral et al. 2010), only copepods above a certain size were fed into both  
268 PCAs. Alternatively, the similarity of studies suggest that copepod morpholog-  
269 ical variation might be well described by these two primary axes. (Sonnet et  
270 al. 2022) used phytoplankton images to investigate how a morphospace could  
271 be used to evaluate community composition changes over time. Comparisons  
272 of copepod morphospaces across temporal and spatial scales may offer a useful  
273 metric for answering biogeographic and ecological questions.

## 274 5.2 Morphology and DVM

275 The pattern of DVM described in this study is consistent with the general night-  
276 time ascent DVM pattern (Bianchi and Mislan 2016; Bandara et al. 2021). The  
277 average vertical profiles display a clear day/night difference (Figure 3). In each  
278 20m depth bin, there was large variation, often exceeding the average concen-  
279 tration. This large variation however, was expected. There can be consider-  
280 able variation between UVP estimates of zooplankton abundance (Barth and  
281 Stone 2022). Additionally, in this study we pooled casts across multiple seasons.  
282 Variability in copepod DVM has been described across seasons (Whitmore and  
283 Ohman 2021). While seasonal variability in DVM is an interesting question  
284 in the Sargasso Sea, the nature of our dataset did not lend itself to this investi-

gation. However, despite the need to pool UVP casts across cruises, the signal of DVM was still observable. Previous studies using in-situ imaging have also noted a signal of DVM with copepods (Pan et al. 2018; Whitmore and Ohman 2021). Yet due to small and uneven sampling, it can be a challenge to quantify DVM using in-situ imaging. As presented in this paper, bin-constrained bootstrapping offers a robust method to quantify WMD and investigate DVM hypotheses.

Consistent with the size-based hypothesis (H1), we documented a clear effect in which larger copepods migrated further. This finding is consistent with several studies which have documented a size-dependent relationship for copepod DVM (Ohman and Romagnan 2016; Aarflot et al. 2019; Pinti et al. 2019). Ohman and Romagnan (2016) noted that moderate-size copepods had the largest migrations. While this may seem contradictory to the present study, the difference between study systems needs be taken into account. The copepods described in the large (high PC1) group had a mean feret diameter of nearly 5mm. Conversely, in Ohman and Romagnan (2016)'s study the "moderate" copepods ranged from 4mm-6mm.

The transparency-based hypothesis (H2) was only supported by patterns within the large copepod group. The large but more transparent copepods (low PC2, high PC1) did not have a detectable DVM signal. Yet the darker copepods (mid and high PC2) had a large DVM signal. Hays (2003) described that copepod pigmentation could explain increased DVM with small ( $<1$ mm) copepods. The lack of a transparency effect for the mid- and low PC1 groups in our study is

surprising. One possibility is that the small, transparent copepods were not well sampled by the UVP (Figure 2). Alternatively, some copepods which do not migrate may have pigmentation to avoid damage from UV radiation. The grey-value recorded in UVP-imaged copepods can be indicative of many features beyond simply pigmentation, notably egg-sacs and gut contents (Vilgrain et al. 2021). Such characteristics vary much more between individuals and can have varied influences on DVM (PEARRE Jr. 2003). Thus the relationship between color and DVM is the result of a delicate balance of minimizing multiple ecological and biological risks (Hansson 2004; Hylander et al. 2014). While well documented, predator avoidance may not always be the primary selective pressure on copepod traits. For example, if the costs of migration are too large for some copepods, they will remain near the surface. However, these copepods then are exposed to UV light and may increase pigmentation to reduce damage.

### 5.3 Conclusion

Overall, our results reveal a complex dynamic between copepod traits and DVM behavior. This study provided new insight into the DVM dynamics in oligotrophic gyres. While many studies have established size as a major trait influencing DVM, investigations into other traits are more limited. Here, we show using in-situ imaging that color/transparency has a major role in DVM behavior, for some sizes of copepods. How size and color influence DVM across seasons and environmental conditions remains a major question. As plankton in-situ imaging tools are used more commonly by oceanographers, larger datasets will

<sup>330</sup> facilitate new investigations.

## <sup>331</sup> **6 Acknowledgements**

<sup>332</sup> Field work for this project was supported by the Bermuda Atlantic Time Series  
<sup>333</sup> Study through NSF OCE 1756105 & NSF OCE 1756312. We would also like  
<sup>334</sup> to thank the BATS research technicians, marine technicians, and crew of the  
<sup>335</sup> R/V Atlantic Explorer. Dr. Ryan Rykaczewski assisted with the initial set-up  
<sup>336</sup> of the UVP. Dr. Leo Blanco-Bercial and Dr. Amy Maas both valuable insight  
<sup>337</sup> and guidance on the analysis.

### <sup>338</sup> **6.1 References**

- <sup>339</sup> Aarflot, J. M., D. L. Aksnes, A. F. Opdal, H. R. Skjoldal, and Ø. Fiksen.  
<sup>340</sup> 2019. Caught in broad daylight: Topographic constraints of zooplankton depth distributions. Limnology and Oceanography **64**: 849–859.  
<sup>341</sup> doi:[10.1002/limo.11079](https://doi.org/10.1002/limo.11079)
- <sup>343</sup> Aksnes, D. L., and A. C. W. Utne. 1997. A revised model of visual range in fish. Sarsia **82**: 137–147. doi:[10.1080/00364827.1997.10413647](https://doi.org/10.1080/00364827.1997.10413647)
- <sup>345</sup> Archibald, K. M., D. A. Siegel, and S. C. Doney. 2019. Modeling the Impact of Zooplankton Diel Vertical Migration on the Carbon Export Flux of the Biological Pump. Global Biogeochemical Cycles **33**: 181–199.  
<sup>346</sup> doi:[10.1029/2018GB005983](https://doi.org/10.1029/2018GB005983)
- <sup>349</sup> Bandara, K., Ø. Varpe, L. Wijewardene, V. Tverberg, and K. Eiane. 2021. Two hundred years of zooplankton vertical migration research. Biological

- 351      Reviews **96**: 1547–1589. doi:[10.1111/brv.12715](https://doi.org/10.1111/brv.12715)
- 352      Barth, A., and J. Stone. 2022. Comparison of an in situ imaging device and  
353      net-based method to study mesozooplankton communities in an oligotrophic  
354      system. Frontiers in Marine Science **9**.
- 355      Bianchi, D., and K. a. S. Mislan. 2016. Global patterns of diel vertical migration  
356      times and velocities from acoustic data. Limnology and Oceanography **61**:  
357      353–364. doi:[10.1002/lno.10219](https://doi.org/10.1002/lno.10219)
- 358      Brierley, A. S. 2014. Diel vertical migration. Current Biology **24**: R1074–R1076.  
359      doi:[10.1016/j.cub.2014.08.054](https://doi.org/10.1016/j.cub.2014.08.054)
- 360      Gorsky, G., M. D. Ohman, M. Picheral, and others. 2010. Digital zooplankton  
361      image analysis using the ZooScan integrated system. Journal of Plankton  
362      Research **32**: 285–303. doi:[10.1093/plankt/fbp124](https://doi.org/10.1093/plankt/fbp124)
- 363      Hansson, L.-A. 2004. Plasticity in Pigmentation Induced by Conflicting Threats  
364      from Predation and Uv Radiation. Ecology **85**: 1005–1016. doi:[10.1890/02-0525](https://doi.org/10.1890/02-0525)
- 365      Hays, G. C. 2003. A review of the adaptive significance and ecosystem conse-  
366      quences of zooplankton diel vertical migrations. Springer Netherlands. 163–  
367      170.
- 368      Hays, G. C., C. A. Proctor, A. W. G. John, and A. J. Warner. 1994. Inter-  
369      specific differences in the diel vertical migration of marine copepods: The  
370      implications of size, color, and morphology. Limnology and Oceanography  
371      **39**: 1621–1629. doi:[10.4319/lo.1994.39.7.1621](https://doi.org/10.4319/lo.1994.39.7.1621)
- 372      Hylander, S., J. C. Grenvald, and T. Kiørboe. 2014. Fitness costs and benefits

374 of ultraviolet radiation exposure in marine pelagic copepods. Functional  
375 Ecology **28**: 149–158. doi:[10.1111/1365-2435.12159](https://doi.org/10.1111/1365-2435.12159)

376 Kelly, T. B., P. C. Davison, R. Goericke, M. R. Landry, M. D. Ohman, and M.  
377 R. Stukel. 2019. [The importance of mesozooplankton diel vertical migration](#)  
378 [for sustaining a mesopelagic food web](#). Frontiers in Marine Science **6**.

379 Maas, A. E., L. Blanco-Bercial, A. Lo, A. M. Tarrant, and E. Timmins-  
380 Schiffman. 2018. Variations in copepod proteome and respiration rate in  
381 association with diel vertical migration and circadian cycle. The Biological  
382 Bulletin **235**: 30–42. doi:[10.1086/699219](https://doi.org/10.1086/699219)

383 Ohman, M. D. 2019. A sea of tentacles: optically discernible traits resolved from  
384 planktonic organisms in situ H. Browman [ed.]. ICES Journal of Marine  
385 Science **76**: 1959–1972. doi:[10.1093/icesjms/fsz184](https://doi.org/10.1093/icesjms/fsz184)

386 Ohman, M. D., and J.-B. Romagnan. 2016. Nonlinear effects of body size and  
387 optical attenuation on Diel Vertical Migration by zooplankton. Limnology  
388 and Oceanography **61**: 765–770. doi:[10.1002/limo.10251](https://doi.org/10.1002/limo.10251)

389 Ohman, M. D., J. A. Runge, E. G. Durbin, D. B. Field, and B. Niehoff.  
390 2002. On birth and death in the sea. Hydrobiologia **480**: 55–68.  
391 doi:[10.1023/A:1021228900786](https://doi.org/10.1023/A:1021228900786)

392 Pan, J., F. Cheng, and F. Yu. 2018. [The diel vertical migration of zooplankton](#)  
393 [in the hypoxia area observed by video plankton recorder](#). IJMS Vol.47(07)  
394 [July 2018].

395 PEARRE Jr., S. 2003. Eat and run? The hunger/satiation hypothesis in vertical  
396 migration: history, evidence and consequences. Biological Reviews **78**: 1–79.

- 397 doi:[10.1017/S146479310200595X](https://doi.org/10.1017/S146479310200595X)
- 398 Picheral, M., S. Colin, and J.-O. Irisson. [EcoTaxa](#), a tool for the taxonomic  
399 classification of images.
- 400 Picheral, M., L. Guidi, L. Stemmann, D. M. Karl, G. Iddaoud, and G. Gorsky.  
401 2010. The Underwater Vision Profiler 5: An advanced instrument for high  
402 spatial resolution studies of particle size spectra and zooplankton. Limnology  
403 and Oceanography: Methods **8**: 462–473. doi:[10.4319/lom.2010.8.462](https://doi.org/10.4319/lom.2010.8.462)
- 404 Pinti, J., T. Kiørboe, U. H. Thygesen, and A. W. Visser. 2019. Trophic in-  
405 teractions drive the emergence of diel vertical migration patterns: A game-  
406 theoretic model of copepod communities. Proceedings of the Royal Society  
407 B: Biological Sciences **286**: 20191645. doi:[10.1098/rspb.2019.1645](https://doi.org/10.1098/rspb.2019.1645)
- 408 Robison, B. H., R. E. Sherlock, K. R. Reisenbichler, and P. R. McGill. 2020.  
409 [Running the gauntlet: Assessing the threats to vertical migrators](#). Frontiers  
410 in Marine Science **7**.
- 411 Schnetzer, A., and D. K. Steinberg. 2002. Active transport of particu-  
412 late organic carbon and nitrogen by vertically migrating zooplankton  
413 in the Sargasso Sea. Marine Ecology Progress Series **234**: 71–84.  
414 doi:[10.3354/meps234071](https://doi.org/10.3354/meps234071)
- 415 Siegel, D. A., T. DeVries, I. Cetinić, and K. M. Bisson. 2023. Quantifying  
416 the ocean’s biological pump and its carbon cycle impacts on global scales.  
417 Annual Review of Marine Science **15**: null. doi:[10.1146/annurev-marine-040722-115226](https://doi.org/10.1146/annurev-marine-040722-115226)
- 418  
419 Sonnet, V., L. Guidi, C. B. Mouw, G. Puggioni, and S.-D. Ayata. 2022. Length,

420 width, shape regularity, and chain structure: time series analysis of phy-  
421toplankton morphology from imagery. Limnology and Oceanography **67**:  
422 1850–1864. doi:[10.1002/lno.12171](https://doi.org/10.1002/lno.12171)

423 Soviadan, Y. D., F. Benedetti, M. C. Brandão, and others. 2022.  
424 Patterns of mesozooplankton community composition and vertical  
425 fluxes in the global ocean. Progress in Oceanography **200**: 102717.  
426 doi:[10.1016/j.pocean.2021.102717](https://doi.org/10.1016/j.pocean.2021.102717)

427 Steinberg, D. K., C. A. Carlson, N. R. Bates, S. A. Goldthwait, L. P. Madin,  
428 and A. F. Michaels. 2000. Zooplankton vertical migration and the active  
429 transport of dissolved organic and inorganic carbon in the Sargasso Sea.  
430 Deep Sea Research Part I: Oceanographic Research Papers **47**: 137–158.  
431 doi:[10.1016/S0967-0637\(99\)00052-7](https://doi.org/10.1016/S0967-0637(99)00052-7)

432 Steinberg, D. K., C. A. Carlson, N. R. Bates, R. J. Johnson, A. F. Michaels,  
433 and A. H. Knap. 2001. Overview of the US JGOFS Bermuda Atlantic  
434 Time-series Study (BATS): a decade-scale look at ocean biology and biogeo-  
435 chemistry. Deep Sea Research Part II: Topical Studies in Oceanography **48**:  
436 1405–1447. doi:[10.1016/S0967-0645\(00\)00148-X](https://doi.org/10.1016/S0967-0645(00)00148-X)

437 Steinberg, D. K., and M. R. Landry. 2017. Zooplankton and the ocean carbon  
438 cycle. Annual Review of Marine Science **9**: 413–444. doi:[10.1146/annurev-marine-010814-015924](https://doi.org/10.1146/annurev-marine-010814-015924)

440 Trudnowska, E., L. Lacour, M. Ardyna, A. Rogge, J. O. Irisson, A. M. Waite, M.  
441 Babin, and L. Stemmann. 2021. Marine snow morphology illuminates the  
442 evolution of phytoplankton blooms and determines their subsequent vertical

443 export. *Nature Communications* **12**: 2816. doi:[10.1038/s41467-021-22994-4](https://doi.org/10.1038/s41467-021-22994-4)

444 Turner, J. 2004. The importance of small planktonic copepods and their roles

445 in pelagic marine food webs.,

446 Vilgrain, L., F. Maps, M. Picheral, M. Babin, C. Aubry, J.-O. Irisson, and S.-D.

447 Ayata. 2021. Trait-based approach using in situ copepod images reveals

448 contrasting ecological patterns across an Arctic ice melt zone. *Limnology*

449 and *Oceanography* **66**: 1155–1167. doi:[10.1002/lno.11672](https://doi.org/10.1002/lno.11672)

450 Whitmore, B. M., and M. D. Ohman. 2021. Zooglider-measured association of

451 zooplankton with the fine-scale vertical prey field. *Limnology and Oceanog-*

452 *raphy* **66**: 3811–3827. doi:[10.1002/lno.11920](https://doi.org/10.1002/lno.11920)

## 453 **7 Data availability statement**

454 All data used in this project are hosted on Ecopart ([https://ecopart.obs-vlfr.](https://ecopart.obs-vlfr.fr/)

455 [fr/](https://ecopart.obs-vlfr.fr/)). Data in its raw form can be accessed from their portal. However, all

456 summary and intermediate data products, as well as code, are publicly available

457 on GitHub ([https://github.com/TheAlexBarth/DVM\\_Migration-Morphology](https://github.com/TheAlexBarth/DVM_Migration-Morphology)).

458 Intermediate data products are formatted as R Data Structure objects, other

459 formats are available on request.

## 460 **8 Supplemental Information**

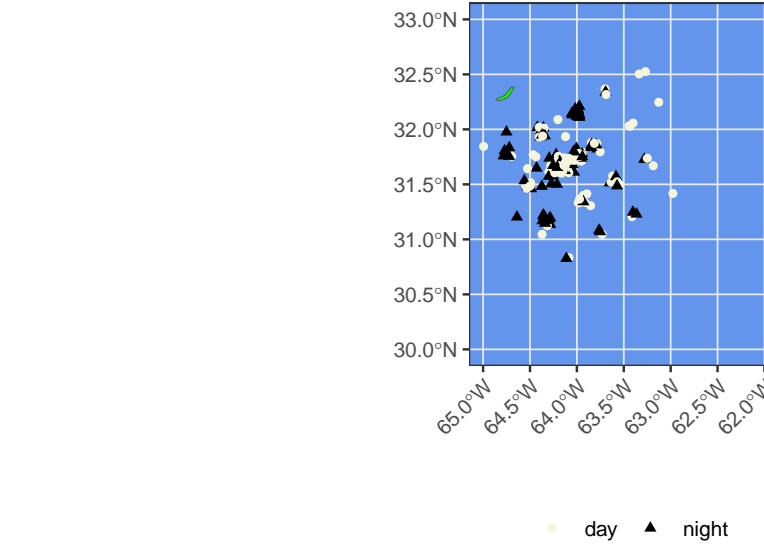


Figure 6: Supplemental Figure S1. Map of CTD Cast Deployments. Dark triangle points indicate night casts, tan circles indicate day casts.

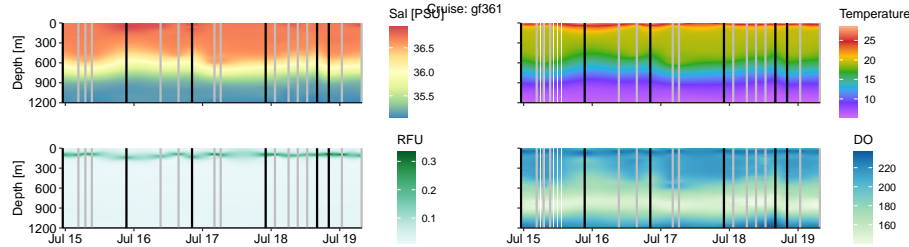


Figure 7: Supplemental Figure S2. Physical parameters across individual cruises. Vertical bars indicate CTD casts events with black indicating night and grey indicating day.

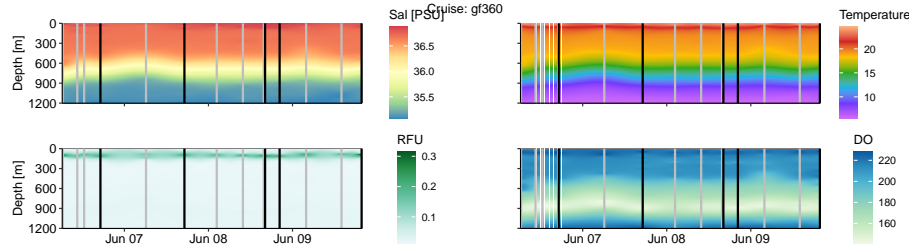


Figure 8: Supplemental Figure S2. Physical parameters across individual cruises. Vertical bars indicate CTD casts events with black indicating night and grey indicating day.

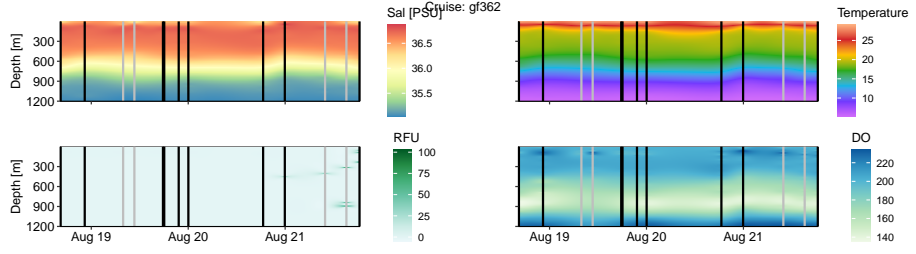


Figure 9: Supplemental Figure S2. Physical parameters across individual cruises. Vertical bars indicate CTD casts events with black indicating night and grey indicating day.

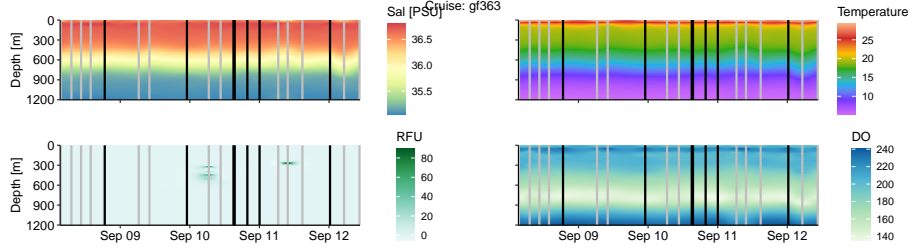


Figure 10: Supplemental Figure S2. Physical parameters across individual cruises. Vertical bars indicate CTD casts events with black indicating night and grey indicating day.

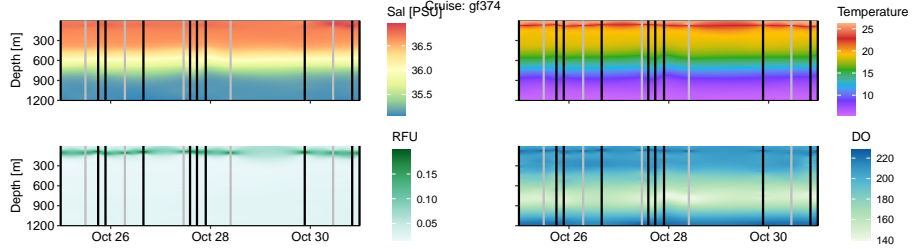


Figure 11: Supplemental Figure S2. Physical parameters across individual cruises. Vertical bars indicate CTD casts events with black indicating night and grey indicating day.

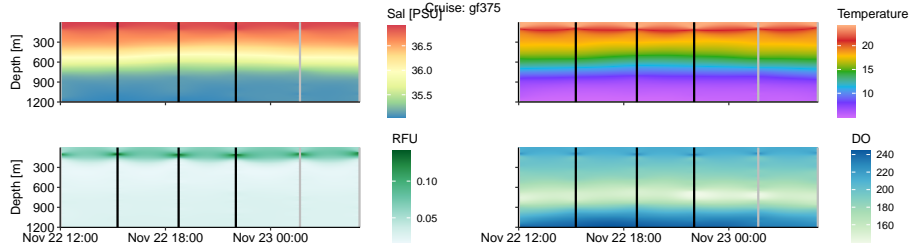


Figure 12: Supplemental Figure S2. Physical parameters across individual cruises. Vertical bars indicate CTD casts events with black indicating night and grey indicating day.

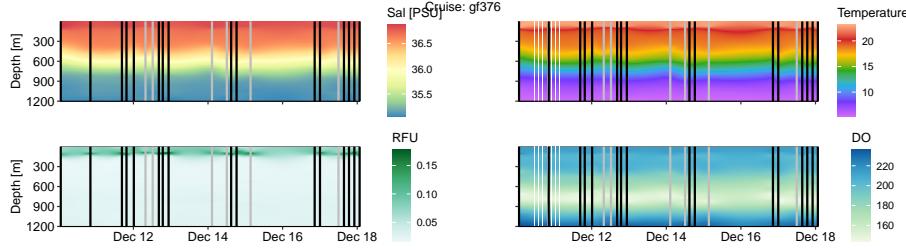


Figure 13: Supplemental Figure S2. Physical parameters across individual cruises. Vertical bars indicate CTD casts events with black indicating night and grey indicating day.

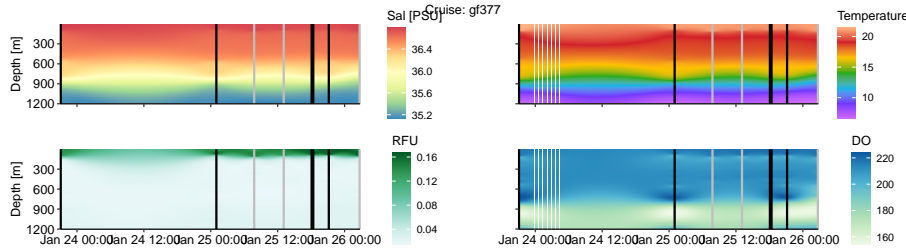


Figure 14: Supplemental Figure S2. Physical parameters across individual cruises. Vertical bars indicate CTD casts events with black indicating night and grey indicating day.

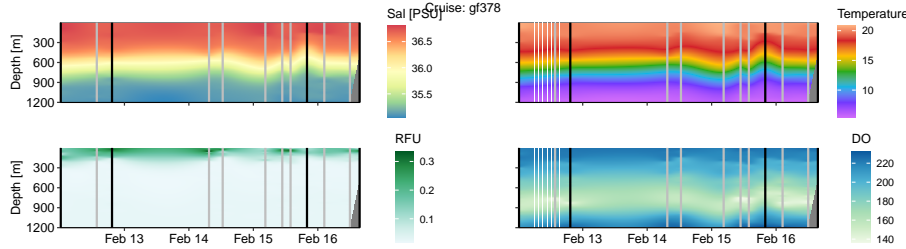


Figure 15: Supplemental Figure S2. Physical parameters across individual cruises. Vertical bars indicate CTD casts events with black indicating night and grey indicating day.

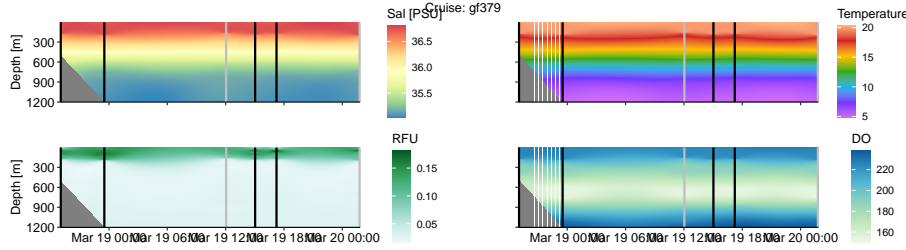


Figure 16: Supplemental Figure S2. Physical parameters across individual cruises. Vertical bars indicate CTD casts events with black indicating night and grey indicating day.

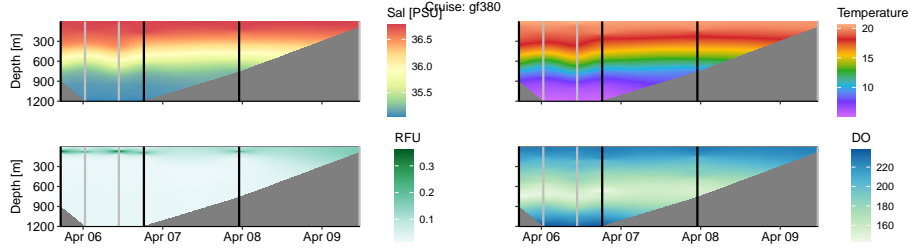


Figure 17: Supplemental Figure S2. Physical parameters across individual cruises. Vertical bars indicate CTD casts events with black indicating night and grey indicating day.

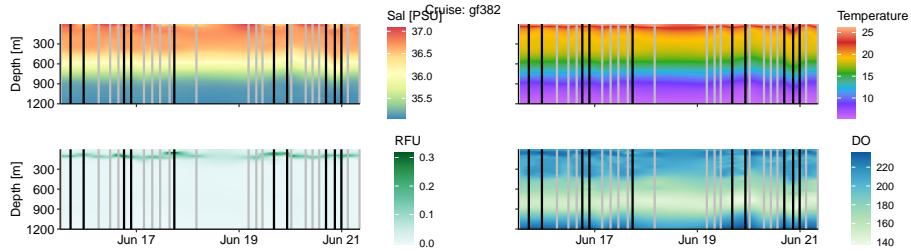


Figure 18: Supplemental Figure S2. Physical parameters across individual cruises. Vertical bars indicate CTD casts events with black indicating night and grey indicating day.

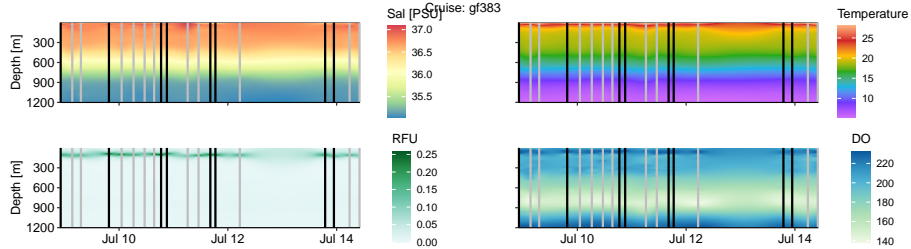


Figure 19: Supplemental Figure S2. Physical parameters across individual cruises. Vertical bars indicate CTD casts events with black indicating night and grey indicating day.

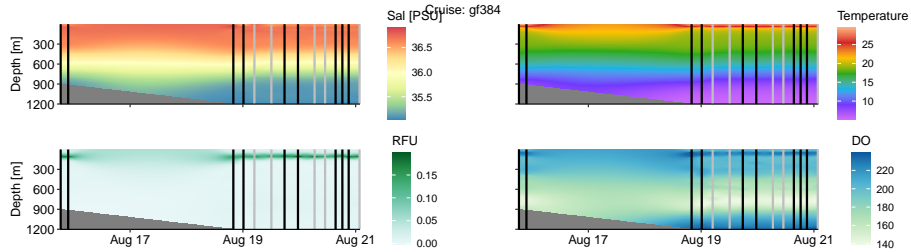


Figure 20: Supplemental Figure S2. Physical parameters across individual cruises. Vertical bars indicate CTD casts events with black indicating night and grey indicating day.

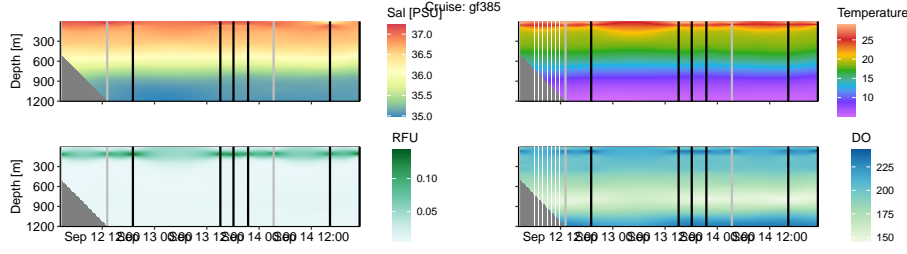


Figure 21: Supplemental Figure S2. Physical parameters across individual cruises. Vertical bars indicate CTD casts events with black indicating night and grey indicating day.

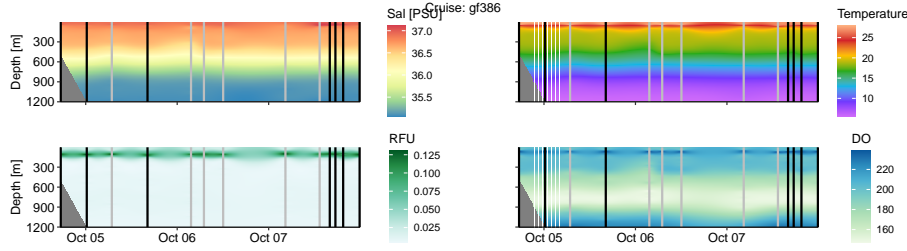


Figure 22: Supplemental Figure S2. Physical parameters across individual cruises. Vertical bars indicate CTD casts events with black indicating night and grey indicating day.

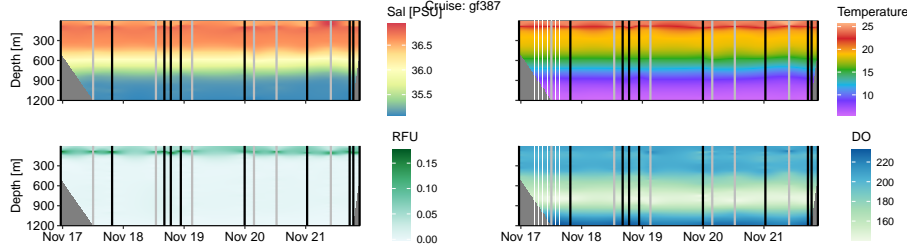


Figure 23: Supplemental Figure S2. Physical parameters across individual cruises. Vertical bars indicate CTD casts events with black indicating night and grey indicating day.

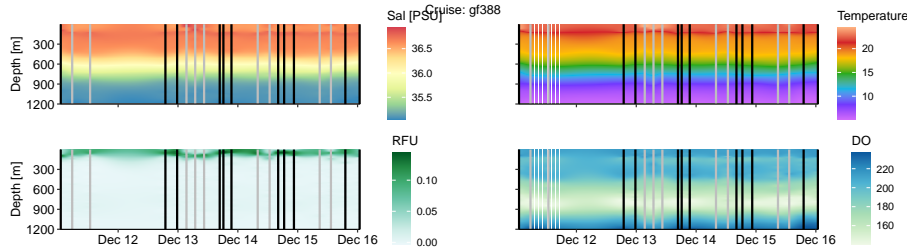


Figure 24: Supplemental Figure S2. Physical parameters across individual cruises. Vertical bars indicate CTD casts events with black indicating night and grey indicating day.

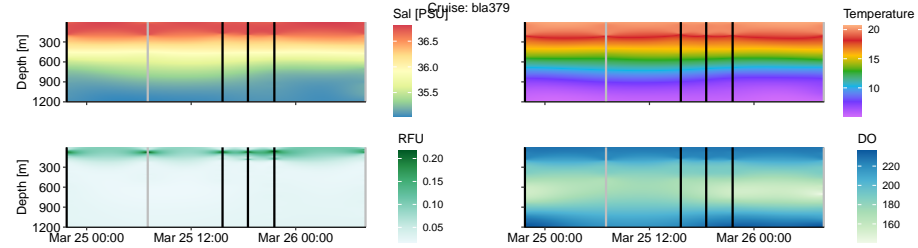


Figure 25: Supplemental Figure S2. Physical parameters across individual cruises. Vertical bars indicate CTD casts events with black indicating night and grey indicating day.

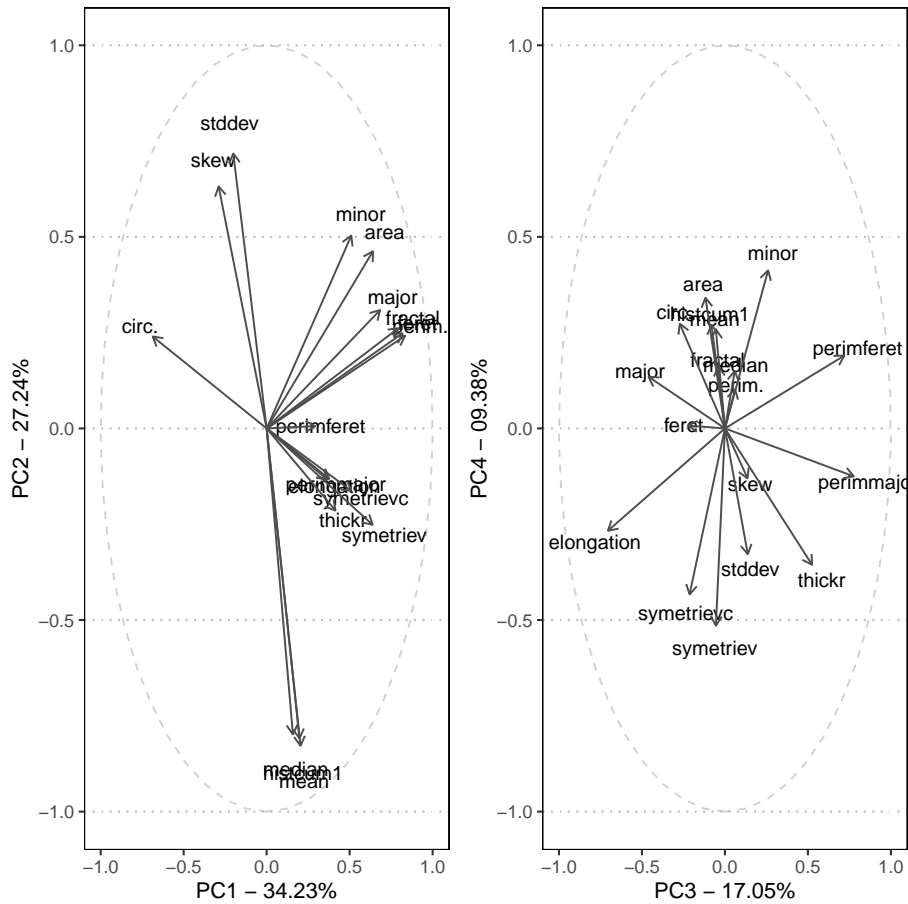


Figure 26: Supplemental Figure S3. PCA plot with major loading variables plotted.

	Dim.1	Dim.2	Dim.3	Dim.4
area	0.7115131	0.5137738	-0.1301928	0.3789753
circ.	-0.7627265	0.2665557	-0.3026239	0.3034329
elongation	0.4080632	-0.1487560	-0.7831847	-0.2965671
feret	0.9096148	0.2756948	-0.2479648	0.0082808
fractal	0.8816770	0.2904962	-0.0440580	0.1793785
histcum1	0.2197180	-0.8987922	-0.0901744	0.3005361
major	0.7593652	0.3432489	-0.5115438	0.1498407
mean	0.2266145	-0.9201880	-0.0611832	0.2875560
median	0.1758116	-0.8872673	0.0657406	0.1668198
minor	0.5668215	0.5593596	0.2891461	0.4585166
perim.	0.9268957	0.2685898	0.0681774	0.1135716
perimferet	0.3251295	0.0068372	0.7989292	0.2111105
perimmajor	0.4183142	-0.1460583	0.8627707	-0.1389696
skew	-0.3216781	0.7017490	0.1514517	-0.1447764
stddev	-0.2234641	0.7971849	0.1531288	-0.3647663
symetriev	0.7091737	-0.2793593	-0.0605051	-0.5720602
symetrievc	0.5673730	-0.1807542	-0.2368157	-0.4811256
thickr	0.4609473	-0.2379533	0.5832035	-0.3954358

<sup>461</sup> Supplemental Table S2. Loading scores for morphological factors on the PCA.